Manuscript title

Evolutionary Assembly and Disassembly of the Mammalian Sternum

Author list

Ava E. Brent¹ Emily A. Buchholtz² Jennifer H. Mansfield¹

Author Affiliation

¹Department of Biology, Barnard College, Columbia University, 3009 Broadway, New York, NY 10027, USA

²Department of Biological Sciences, Wellesley College, 106 Central St., Wellesley, MA 02481, USA

Lead Contact

Emily A. Buchholtz ebuchholtz@wellesley.edu

ORCID identifiers

Ava E. Brent: 0000-0002-8670-5188 Emily A. Buchholtz: 0000-0002-8241-2388 Jennifer H. Mansfield: 0000-0001-6019-0668

Summary

Evolutionary transitions are frequently associated with novel anatomical structures¹, but the origins of the structures themselves are often poorly known. We use developmental, genetic, and paleontological data to demonstrate that the therian sternum was assembled from preexisting elements. Imaging of the perinatal mouse reveals two paired sternal elements, both composed primarily of cells with lateral plate mesoderm origin. Location, articulations, and development identify them as homologs of the interclavicle and the sternal bands of synapsid outgroups. The interclavicle, not previously recognized in therians², articulates with the clavicle and differs from the sternal bands in both embryonic HOX expression and pattern of skeletal maturation. The sternal bands articulate with the ribs in two styles, most clearly differentiated by their association with sternebrae. Evolutionary trait mapping indicates that the interclavicle and sternal bands were independent elements throughout most of synapsid history. The differentiation of rib articulation styles and the subdivision of the sternal bands into sternebrae were key innovations likely associated with transitions in locomotor and respiratory mechanics^{3,4}. Fusion of the interclavicle and the anterior sternal bands to form a presternum anterior to the first sternebra was a historically recent innovation unique to therians. Subsequent disassembly of the radically reduced sternum of mysticete cetaceans was element-specific, reflecting the constraints that conserved developmental programs exert on composite structures.

Results and Discussion

The sternum of therian mammals plays key roles in feeding, locomotion, and respiration, but it did not exist as a discrete structure in their early synapsid ancestors. In these ancestors, the ventral pectoral girdle was dominated by the clavicle-articulating interclavicle (IC). In contrast, both the clavicle and the thoracic ribs articulate with the sternum in therians, traditionally identified as the developmental fusion product of the sternal bands (SBs); the IC is not recognized. This interpretation implies that ancestral muscular and skeletal interactions with the IC were lost and then were secondarily re-established with the SBs. Alternatively, the sternum may have been assembled from independent IC and SB elements that were secondarily integrated into a single structure (e.g., 4-6).

Four lines of evidence identify that the sternum is an assembled structure and allow a preliminary reconstruction of its evolutionary history. First, two elements with different developmental histories are described in the presterna of fetal and postnatal mice. They are homologized with the IC and the SBs of outgroups. Second, structural and developmental differences in rib/sternum articulation style identify the anterior and posterior SBs as two partially independent patterning units. Third, evolutionary mapping of sternal traits is used to reconstruct the history of sternal assembly in fossil synapsids. Finally, the path of radical sternal reduction in baleen whales is reconstructed and shown to reflect the stepwise loss of developmentally defined elements. Coupled with previously documented and regionally restricted phenotypes in mice, these results indicate that the ancestral sternal elements retained independent developmental identities during their incorporation into the sternum.

Sternal element identification and development

In most tetrapods, the IC and SBs are separate skeletal elements that articulate with the clavicles and the ribs, respectively. The interclavicle and clavicle predate the origin of tetrapods and are thought to have ancestry in dermal body armor^{7–9}. In contrast, the SBs evolved within stem tetrapods, and derive from the lateral plate mesoderm (LPM) of the forelimb field¹⁰. The conservatism of structural interactions and developmental programs suggests the possibility that

the therian presternum is a composite structure, containing both the IC and the anterior portion of the SBs, here designated as the anterior SBs (ASB). The more posterior portion of the SBs (the PSB) constitutes the traditionally recognized mesosternum. External evidence for multiple presternal elements is rare. Transitions in bone texture and internal boundaries occur just anterior to the T1 rib articulation in some basal therians, notably xenarthrans⁴. Here, imaging in perinatal and adult mice confirms a composite presternum. At postnatal day (P2), two distinct elements were observed by immunofluorescence for Tenascin, an extracellular matrix component of cartilage, bone, and connective tissue (Figure 1A-F; Figure S1). These are labelled IC and ASB, respectively, with arguments for their homology to the interclavicle and the anterior portion of the sternal bands given below. The anterodorsal IC and posteroventral ASB overlap anterior to the first thoracic (T1) rib articulation (Figure 1A-B; Figure S1E), but are always distinct, each bounded by its own connective tissue. These observations are consistent with previous reports of two bilateral condensations in the embryonic presternum of mouse and human^{5,6}.

Viewed in frontal sections, the IC is small, bilateral and articulates with the medial ends of the clavicles (Figure 1A,C; Figure S1A). A tendinous attachment is made to the sternal head of the sternocleidomastoid muscles (arrows in Figure 1C and Figure S1Aiv, Fiv). Progressing ventrally in frontal views (Figure 1B, D, J; Figure S1B-C), or in sagittal views (Figure 1E, F, K; S1D-G), the IC abuts the ASB, a second bilateral, elongated element that articulates with the somitederived (Meox1-Cre-RFP-labeled) T1 ribs laterally (Figure 1D; S1Biv), the sternocleidomastoid muscle anteriorly (arrows in Figure 1D, F; Figure S1Biv, Fiv, Giv), the pectoralis major muscle ventrally, and the infrahyoid muscles dorsally. The ASB are continuous with the posterior sternal bands (PSB), which exhibit an AP series of sternebral ossification centers between the rib attachments (Figure S1C-G). Lineage-labeling for lateral plate mesoderm derivatives (with Prx1-Cre-RFP, Figure S2A-B) or for somite derivatives (with Meox1-Cre-RFP, Figure 1, Figure S2C-D) reveals that the IC and ASB are both composed predominantly of LPM-derived cells⁵.

Two lines of evidence indicate that the IC and SB are under independent developmental control. First, they differ in the timing of skeletal development. Both embryonic condensations express chondrocyte marker SOX9, although expression is more diffuse in the IC compared with the SB (Figure S2Hi, viii and ⁵). As previously described, the SB undergo endochondral ossification during fetal development, ossifying by E18.5 except at positions of sternebral joint formation (Figure S3A-F). In contrast, only the posterior portion of the IC condensation undergoes endochondral ossification, and this is delayed until after birth. The posterior IC chondrifies by P10 (Figure S3G-H but ossifies only in adults (Figure S3I). The SB and IC also appear to undergo differential growth, because their anlagen occupy similar space in embryonic sections (Figure 1G), but the ASB dominates the presternum during postnatal development.

The IC and ASB are additionally distinguished by embryonic HOX expression. In E14.5 mice, HOXA5 is expressed in the ASB anterior to and including the T1 rib attachment, but HOXA5 is not expressed in the IC (⁵ and Figure 1G, Figure S2E, F, Hi-Ji). In contrast, HOXB4 expression is robust throughout the IC and ASB (Figure 1G; S2H). Together, the presence of identifiable developmental units, the dramatic difference in skeletal maturation, and the unique molecular identities, all indicate that the IC and ASB are distinct elements under independent developmental control.

Arguments for homology are classically based on similarities of position, articulation, muscle connectivity, and development (e.g., 11-14). These lines of evidence support an identification of the paired anterior element as the homolog of the interclavicle. Like the interclavicle of monotremes and more distant outgroups (e.g., 15,16 and Fig. 1H), the anterior element of the

mouse lies in the ventral midline, articulates with the medial ends of the clavicles anterolaterally (Figure 1A, D, J) and overlaps dorsal to the SB posteriorly (Figure 1C, F, K). Also like the IC, it lacks rib articulations. Additionally, the sternocleidomastoid muscle inserts on the anterior element (Figure 1A,C) as it does on the interclavicle in *Sphenodon*¹⁷, *Iguana*¹⁸, and a wide range of turtles¹¹. In monotremes, the sternomastoid muscle inserts on the IC as well as on more posterior parts of the sternum¹⁹, which is also observed in mice (Figure 1). The association between the sternocleidomastoid and the interclavicle is additionally predicted by the muscle connectivity hypothesis for gill arch-derived muscles¹².

Both the clavicle and IC have dermal bone components and also contain endochondral portions in living mammals^{15,20}. In monotremes, the interclavicle develops from paired, lateral commashaped dermal bones (*pars desmalis interclaviculae*) and a midline endochondral pro-osteon²¹ or *pars chondralis interclaviculae*^{15,22}. The mouse IC resembles this in that it contains internal subdivisions, including an endochondral component. The anterolateral (clavicle-articulating) region of the mouse IC condenses and expresses SOX9 as well as connective tissue markers such as Tenascin, and stains weakly with Alcian blue, but does not chondrify or mineralize consistent with a connective tissue identity. In contrast, the posteromedial portion of the IC that overlaps the ASB is endochondral, as it is in monotremes, except that in mice it does not chondrify until after birth (P10) and does not ossify until after postnatal day 30. The presence of additional components homologous to other pectoral girdle elements (such as the procoracoid, proposed present in the marsupial sternum^{8,22}) cannot be ruled out.

The posterior element of the mouse presternum can be identified as the anterior portion of the SBs (ASB) based on multiple criteria. SBs originate from LPM in the axillary region of the forelimb bud. Their subsequent migration to the midline and fusion has been documented in both mouse and chick (e.g., 10,23–25). Like the SBs, the mouse ASB is clearly paired (Figure 1C, G), and is of LPM origin (Figure S2). Like the SBs, it articulates with the ribs (Figure S1C), and is continuous with the PSBs of the mesosternum. It further undergoes endochondral ossification with the same timing as the PSB (Figure S3A-G). Based on these features, the posterior element of the presternum almost certainly derives from the SBs as previously proposed 1,6,26. Taken together, although the adult therian sternum appears externally subdivided into presternum and mesosternum, its development indicates that its main subdivision is instead between the IC and the SB within the presternum.

Rib articulation style and sternal band regionalization

The therian presternum and mesosternum differ in the style of their rib articulations. The T1 joint is traditionally described as a synchondrosis.²⁷ In adult mice, the distal T1 rib tip bifurcates, and the synchondrosis consists of a thin cartilaginous connection between the more anterior rib tip and the presternum (Figures 2A and S3J, Ki-ii). The presternum is fully ossified at the T1 articulation. In contrast, T2 and more posterior ribs join the mesosternum at synovial joints²⁸. However, in mice these distal ribs also retain a thin cartilaginous connection to the sternum at anteroventral articular surfaces of the joints (Figure 2A and Figure S3Kiv, arrow). Thus, all ribs thus retain a direct skeletal connection to the sternum, but sternal morphology differs dramatically at T1.

- 147 The unique nature of the T1 costosternal attachment could derive from regionalized
- developmental processes within the ribs, the SB, or both. Interestingly, the embryonic SB differ
- molecularly at the T1 versus more posterior rib articulations. HOXA5 is expressed in rib
- chondrocytes, perichondrium, and distal rib tips of both T1 and T2 (Figure 2B-C; Figure S2I-J;
- and see ⁵). HOXA5 is also expressed in both the chondrocytes (Figure 2B, yellow arrow, and
- Figure S2I) and perichondrium of the ASB. Thus, its expression spans the attachment of somite-

- derived T1 ribs, LPM-derived rib perichondrium, and LPM-derived ASB that form the first
- 154 costosternal attachment. In contrast, HOXA5 is not expressed in PSB at the T2 articulation
- 155 (Figure 2C and Figure S2J), where HOXB4 is expressed instead (Figure S2J).
- Hox expression differences between the ASB and PSB suggest that a regionalized response
- 157 could play a role in costosternal attachment style. Embryonic rib anlagen are known to induce
- sternebral joint formation via an unknown signal²⁹ but the developmental difference that
- prevents this at T1 is unknown. In mouse, sternebra-associated ribs contrast with both mouse
- T1 rib and all avian ribs (all of which lack sternebrae) in the embryological origin of their distal
- perichondrium in somites versus LPM^{30,31}. This difference has also been described as a
- difference in the position of the lateral somitic frontier (LSF), an embryonic morphological border
- between somite and LPM-derived tissues that is an important site for the integration of
- patterning information (reviewed in ³²). The functional role of LSF position in rib articulation style
- has not been tested, but if it is determined to be causative, then morphological observations
- alone could be used as a proxy to predict LSF position in non-model taxa, and to trace changes
- alone could be used as a proxy to predict LSF position in non-model taxa, and to trace changes
- in LSF position over evolutionary time. HOXA5 costosternal expression described above does
- not appear to track with the LSF but instead is expressed across this boundary.

169 170

171

172173

174

175

Genetic evidence from mouse further supports the interpretation of ASB and PSB as partially independent patterning units. Several loss-of-function phenotypes differentially affect the growth of these regions, including *Hox4-6* genes³³, *Sox9*³⁴, and *Tgfß2*³⁵. Further, *Tbx5* heterozygous mice show a transformation in which the sternum segments at the T1 joint³⁶. *Tbx5* is expressed primarily in the forelimb field and its derivatives, which are LPM-derived, further suggesting that LPM is a key source of patterning information. Together these demonstrate genetic separability of the ASB and PSB and support the possibility of divergent evolutionary paths.

176 177 178

179

180

181

182

183

Finally, although interactions between somite-derived rib anlagen and LPM-derived SBs appear largely conserved and are considered a shared feature of tetrapod embryos, adult skeletal structures vary. For example, ossified SBs were apparently lost and re-established early in the synapsid lineage (see below). Interestingly, it was recently shown that much of the therian pectoralis major muscle, which articulates with the ossified SB, is not homologous to that of other amniotes and instead has a different embryonic origin³⁷, suggesting a relatively recent and possible co-evolution of skeleton and muscle.

184 185 186

Assembly and disassembly of sternal elements.

The presence of two major elements and of two different rib articulation styles in the therian sternum indicates a complex history of assembly to which the fossil record offers insight.

188 189 190

191

192

187

Synapsids underwent significant ecological and morphological diversification during a history of more than 300 million years (e.g., ^{38–40}). This diversification is also reflected in sternal structure. Synapsid sternal diversity is simplified here by grouping variants into four general anatomical categories (Fig. 3).

193 194 195

196 197

- (1) Independent IC, but no ossified sternal bands or plate:
- The ventral limb girdle is composed of only a T-shaped IC that articulates broadly with the clavicles. Although sternal band anlagen may have been present, they were not ossified or preserved.

198 199 200

- (2) Independent IC and ossified sternal plate, but no sternebrae:
- The IC is robust and often broadly T-shaped. An undivided midline sternal plate lies posterior to, or sometimes overlaps, the IC ventrally. In some specimens, rib

articulations can be inferred from thickenings on the plate margins, but there are no sternebrae.

(3) Independent IC and ossified sternum with sternebrae: The interclavicle is a relatively small independent element, and in some specimens its posterior ramus lies between the anterior tips of the SBs in the midline. The sternum is subdivided into sternebrae, whose boundaries occur at all rib/sternal joints except for T1.

(4) Ossified sternum with sternebrae; an independent IC is absent: The sternum is subdivided into an anterior presternum that articulates with the clavicle and the T1 rib and a posterior mesosternum + xiphisternum that articulates with the posterior ribs. Sternebral boundaries occur at all rib/sternal joints except for T1.

Mapping sternal anatomical categories onto a consensus synapsid phylogeny inferred from other traits allows reconstruction of events in sternal evolution (Figure 3) and signals points of possible functional transition. This analysis indicates that the IC and the SBs were originally independent structures in basal synapsids (Figure 3A, "pelycosaurs"; see also ³), as the differences in their developmental programs predict. Anteriorly, the ancestral IC almost certainly provided attachment sites for the infrahyoid and sternomastoid muscles⁴¹ as it does in living monotremes¹⁹. The musculature of the forelimb (e.g., *m. pectoralis*) and the abdomen (e.g., *m. rectus abdominus*) likely took origin from its posterior ramus^{42–44}.

Ossified SB elements are first known from the subsequent radiation of non-mammalian (basal) therapsids (Figure 3B), which show diverse pectoral appendage size and anatomy³⁹. The addition of an ossified sternal plate posterior to the interclavicle likely provided more posterior and/or more robust attachment sites for pectoral and abdominal muscle groups. It is interpreted here as facilitating early stages of the postural transition of the forelimb from a sprawling to a more paraxial orientation that is predicted by glenoid fossa shape^{42,45}. Therapsid sternal plates also provided fixed articulation sites (likely synarthroses) for multiple ribs, implying that these typically large animals had robust and rigid ribcages.

The subsequent appearance of sternebrae in basal cynodonts (Figure 3C), and also recently identified in a Permian gorgonopsian^{3,46}, marks the differentiation of the SBs into an ASB without sternebrae and a PSB with sternebrae. The taxonomic restriction of sternebrae to late-branching taxa identifies stenebral presence as derived relative to sternebral absence. This innovation also signals a major transition to a regionally differentiated ribcage that was both stable and flexible. Anteriorly, the T1 synarthrosis with the ASB provided an anchor for the forelimb; posteriorly, moveable rib joints with the PSB and between adjacent sternebrae indicate a ribcage that was capable of expansion during ventilation (e.g., ^{28,47–49}). Where documented in living mammals (human, dog), costal contributions to changes in ribcage volume are synergistic with those caused by the diaphragm⁵⁰. Sternebrae are therefore a possible proxy for the presence of a muscularized diaphragm in fossil taxa (see also ³).

The integration of the ASB and the IC into a composite presternum across a developmental discontinuity occurs only in therian mammals (Figure 3D); the boundary between the presternum and the mesosternum occurs within the SBs. In humans, this boundary (the sternal angle) is a pliable cartilaginous hinge joint that increases in angular magnitude during deep inspiration. Its postulated role is to store energy during inspiration, and release it during exhalation, enhancing ribcage deflation⁵¹. Action of the sternal angle joint in other mammals, fossil and extant, is unknown.

The radical reduction of the sternum in mysticete (baleen) whales presents a unique opportunity to observe the evolutionary pattern of sternal disassembly. Basal mysticetes were toothed raptors, and sternal reduction occurred coincident with their transition to bulk feeding (e.g., ^{52–56}).

The sterna of basal mysticetes closely resemble those of terrestrial mammals with the exception that (like all cetaceans) they lack a clavicle. For example, the late Eocene toothed mysticete *Mystacodon* (⁵⁷ and Figure 3E) had characteristic presternal sites for the T1 rib articulations and posterior hemifacets for the T2 rib. Multiple mesosternal sternebrae and a xiphisternum indicate the presence of numerous posterior sternal ribs. Both the dentition and the sternal anatomy of *Mystacodon* suggest that the feeding transition had not yet occurred.

The sterna of more crownward mysticetes exhibit two opposing trends: the presterna are robust and often expanded in relative size, whereas the mesosternum and the number of sternal ribs is reduced. Both toothed (e.g., ⁵⁵) and toothless (e.g., ⁵⁸) fossil mysticetes that bridge the raptorial to bulk feeding transition have presterna with large precostal areas, the attachment site for infrahyoid muscles. These muscles retract the tongue in living suction feeders (e.g., *Eschrichtius*⁵⁹), providing a possible explanation for the retention of the interclavicle despite absence of the clavicle.

Sterna of the Late Oligocene mammalodont *Mammalodon*⁶⁰ and the basal chaeomysticetes *Sitsqwayk* (⁵⁸ and Figure 3F) and *Maiabalaena*⁵⁶ had facets for both the T1 and T2 ribs, indicating the existence of at least one mesosternal sternebra and rib. Sterna completely lacking the mesosternum (PSB) and articulating only with the T1 rib are known as early as the Late Oligocene (e.g., in the eomysticete *Waharoa* ⁶¹), as well as in the extinct cetotheres (e.g., ^{62,63}) and in all living balaenids (Figure 3G) and neobalaenids.

The progressive loss of posterior rib articulations and the PSB that began early in the raptorial to bulk-feeding transition likely facilitated increased thoracic compression, which counters lung compression and reduced intrathoracic pressure at depth in living taxa (e.g., ^{64–69}) as does the associated absence of double-headed ribs at rib/vertebral articulation sites ⁷⁰. Although the feeding depth of fossil taxa is unknown, most living filter feeding mysticetes forage at depth despite its significant energetic costs and respiratory challenges (e.g., ^{71,72}).

The final step in disassembly of the mysticete sternum occurs in balaenopterids, lunge-feeding giants that engulf huge volumes of water and evasive prey into a massively expandable ventral buccal pouch (e.g., 73). Balaenopterids (Figure 3H) are unique among therians in the complete absence of osteological articulations between the ribs and the sternum. A paucity of specimens of these huge animals and the extreme difficulty of dissecting those that are recovered have led to disparate reconstructions of the relationship between the T1 ribs and the sternum. Embryonic specimens (e.g., 74 and Figure S3L) demonstrate definitively that the distal tips of the T1 ribs lie posterior to the lateral sternal wings, surrounded by soft tissue. There are no facets for T1 articulation on the body of the sternum. This anatomy is interpreted here as indicating that the SBs (i.e., not only the PSB but also the ASB) are entirely absent, and that the sole remaining element of the balaenopterid "sternum" is the IC. Because the body wall becomes less compliant with size 75, adaptations that enhance thoracic compression are especially critical in these giant animals 67,76, as external pressures can reach 2,000 kPa at foraging depths 77.

In summary, the identification of the ancestral interclavicle in living therians demonstrates that the sternum is an assembled structure. The IC and SB of living taxa exhibit independent developmental programs and have retained ancestral skeletal articulations with the clavicle and the ribs, despite their assembly into a larger structure. The same independent developmental

programs have allowed independent element assembly, modification, and loss, facilitating novel responses to changing selection pressures.

Acknowledgements

We thank Juha Partanen (University of Helsinki) for the *Meox1-Cre* mouse line and Jeremy Dasen (New York University), for the HOXA5 antibody. The HOXB4 antibody was obtained from the Developmental Studies Hybridoma Bank, created by the NICHD of the NIH and maintained at The University of Iowa, Department of Biology, Iowa City, IA 52242. Research in the Mansfield lab is funded by NSF IOS-2019537, and acquisition of a confocal microscope at Barnard by an NSF MRI award (DBI-1828264). Tom French, Mark Uhen, John Ososky, Nicholas Pyenson, Sara Ketelsen, Eleanor Hoeger, Christian Sidor, Katherine Anderson, Christian de Muizon, Mark Omura, Byron Freeman, Nikki Castelberry, Nicole Pontzer, Jeff Bradley, and Katherine Doyle all provided access to specimens under their care. Christian de Muizon, Pavel Gol'din, Bobby Boessenecker, Angie Batson, and Jamie Jesanis provided access to photos and articles. We thank Claire Siege and Paula Hopper for data collection assistance.

Author Contributions

Investigation, A.E.B., E.A.B., and J.H.M.; Writing – Original Draft, A.E.B., E.A.B., and J.H.M.; Writing – Review & Editing, A.E.B., E.A.B, and J.H.M.; Visualization, A.E.B., E.A.B. and J.H.M.; Funding Acquisition, J.H.M.; Resources, A.E.B., E.A.B, and J.H.M. All authors contributed equally to the project and are listed alphabetically.

Declaration of Interests

The authors declare no competing interests.

STAR Methods

RESOURCE AVAILABILITY

338 Lead contact

Further information and requests for resources and reagents should be directed to and will be fulfilled by the lead contact, Emily Buchholtz (ebuchholtz@wellesley.edu).

Materials availability

This study did not generate new unique reagents.

Data and code availability

All data reported in this paper will be shared by the lead contact upon request. This paper does not report original code.

EXPERIMENTAL MODEL AND SUBJECT DETAILS

- The following mouse lines were used: Prx1-Cre: B6.Cg-Tg(Prrx1-cre)1Cjt/J
- 351 (RRID:IMSR_JAX:005584)81; Rosa6tdtomato; B6.Cg-Gt(ROSA)26Sortm9(CAG-tdTomato)Hze/J
- 352 (RRID:IMSR JAX:007909)82; Meox1Cre: Meox1tm1(cre)Jpa83. Wild-type specimens for skeletal
- analysis were generated from a strain on the 129S/SvEv-Gpi1 background or from mixed
- 354 129/B6 backgrounds. Adult skeletal morphology in adults was visualized in specimens from
- 355 129S, B6 and mixed backgrounds and did not vary across these strains. Crosses to generate

356 RFP-labeling and genotyping of mice was carried out as previously described⁵. All procedures 357 were performed in accordance with the NIH Guide for Care and Use of Laboratory Animals and 358 approved by the Columbia University IACUC.

359 360

361

362 363

364

365

METHOD DETAILS

Mouse crosses and genotyping

Crosses and genotyping were performed as previously described⁵. Briefly, genetic lineage labeling was performed by crossing a male harboring a Cre allele (Meox1-Cre or Prx1-Cre) to a female carrying a Cre-activated RFP transgene. Genotyping of tail-snip DNA was performed with primers for Cre or RFP. Genotyping primers (5' to 3'): Cre forward

366 GAACCTGATGGACATGTTCAGG, reverse AGTGCGTTCGAACGCTAGAGCCTGT; 367

tdTOMATO/RFP forward CTGTTCCTGTACGGCATGG, reverse

GGCATTAAAGCAGCGTATCC. Timed-pregnant females were sacrificed and embryos expressing the fluorescent reporter were collected at the stages indicated.

369 370 371

372

373 374

375

376

377

378 379

380

368

Skeletal staining and histology

Whole-mount Alcian Blue and Alizarin Red staining on whole-mount specimens was performed as previously described⁸⁴. For section histology, 10µm paraffin sections were prepared as previously described⁸⁵ with the addition of a decalcification step for specimens at or older than P14. For decalcification, fixed tissue was incubated in 20% EDTA at 4°C for 1-2 weeks prior to paraffin embedding as usual. For section Alcian blue staining, slides were baked and rehydrated to dH₂0, incubated 5-10 minutes in 1% Alcian blue 8GX, 3% acetic acid, washed in dH₂0 and mounted in gelvatol⁸⁵. For section Alizarin red staining, baked, rehydrated slides were incubated for 1.5 minutes in 0.67% Alizarin red S in dH₂0 (pH4.2), washed in dH₂0 and mounted in gelvatol. Hematoxylin and eosin staining was performed with a kit (Abcam ab245880) following manufacturer's instructions.

381 382 383

384 385

386

387

Immunofluorescence

Immunostaining was performed as previously described⁵. Primary antibodies: HoxA5 (⁸⁶; 1:5000); HoxB4 (87; 1:00); Sox 9 (Millipore-Sigma AB5535, 1:500 or RnD Systems AF3075-SP 1: 500); RFP (Chromotek 5F8, 1:1000 or Rockland 600-401-379, 1:200); muscle Actin My32 (Sigma M4276, 1:250); Tenascin (Sigma-Aldrich T3413, 1: 100). Secondary antibodies: Alexa-488, 594, or 647-conjugated secondary antibodies (Jackson Immunoresearch, diluted 1:400).

388 389 390

391

392

Museum acronyms:

USNM, National Museum of Natural History, Washington, D.C.

MCZ, Museum of Comparative Zoology, Cambridge, MA

UWBM, Burke Museum of Natural History, University of Washington, Seattle, WA

393 394 395

KEY RESOURCES TABLE

(Uploaded as a separate WORD file).

396 397 398

399

400

401

402

403

References

- Jacob, F. (1977). Evolution and tinkering. Science 196, 1161–1166. 10.1126/science.860134.
- Luo, Z.-X. (2015). Origin of the Mammalian Shoulder. In Great Transformations in 2. Vertebrate Evolution, K. P. Dial, N. H. Shubin, and E. L. Brainerd, eds. (University of Chicago Press), pp. 167–187. 10.7208/chicago/9780226268392.003.0010.
- 404 Bendel, E.-M., Kammerer, C.F., Luo, Z.-X., Smith, R.M.H., and Fröbisch, J. (2022). The 3. 405 earliest segmental sternum in a Permian synapsid and its implications for the evolution of

- 406 mammalian locomotion and ventilation. Sci Rep *12*, 13472. 10.1038/S41598-022-17492-407 6.
- 408 4. Buchholtz, E.A., Yozgyur, Z.M., Feldman, A., Weaver, A.A., and Gaudin, T.J. (2020). The therian sternum at the lateral somitic frontier: Evolution of a composite structure. J Zool 315, 19–28. 10.1111/jzo.12809.
- Mitchel, K., Bergmann, J.M., Brent, A.E., Finkelstein, T.M., Schindler, K.A., Holzman,
 M.A., Jeannotte, L., and Mansfield, J.H. (2022). Hoxa5 Activity Across the Lateral Somitic
 Frontier Regulates Development of the Mouse Sternum. Front Cell Dev Biol *10*, 806545.
 10.3389/FCELL.2022.806545.
- 415 6. Rodríguez-Vázquez, J.F., Verdugo-López, S., Garrido, J.M., Murakami, G., and Kim, J.H. (2013). Morphogenesis of the manubrium of sternum in human embryos: a new concept. Anat Rec 296, 279–289. 10.1002/ar.22623.
- 418 7. Grom, K., Pasicka, E., and Tarnawski, K. (2016). Comparative anatomy of pectoral girdle 419 and pectoral fin in Russian sturgeon and American paddlefish. Folia Morphologica 420 (Poland) 75, 173–178. 10.5603/FM.a2015.0093.
- Vickaryous, M.K., and Hall, B.K. (2006). Homology of the reptilian coracoid and a reappraisal of the evolution and development of the amniote pectoral apparatus. J Anat 208, 263–285. 10.1111/J.1469-7580.2006.00542.X.
- 424 9. Romer, A.S. (1957). Osteology of the Reptiles (University of Chicago Press).
- 425 10. Feneck, E.M., Bickley, S.R.B., and Logan, M.P.O. (2021). Embryonic development of the avian sternum and its morphological adaptations for optimizing locomotion. Diversity (Basel) *13*, 481. 10.3390/d13100481.
- 428 11. Lyson, T.R., Bhullar, B.A.S., Bever, G.S., Joyce, W.G., de Queiroz, K., Abzhanov, A., and Gauthier, J.A. (2013). Homology of the enigmatic nuchal bone reveals novel reorganization of the shoulder girdle in the evolution of the turtle shell. Evol Dev *15*, 317–325. 10.1111/ede.12041.
- 432 12. Matsuoka, T., Ahlberg, P.E., Kessaris, N., Iannarelli, R., Dennehy, U., Richardson, W.D., McMahon, A.P., and Koentges, G. (2005). Neural crest origins of the neck and shoulder. Nature *436*, 347–355. 10.1038/nature03837.
- 435 13. Raff, R.A. (1996). The Shape of Life (The University of Chicago Press) 10.7208/chicago/9780226256573.001.0001.
- 437 14. Vickaryous, M.K., and Hall, B.K. (2010). Comparative development of the crocodylian interclavicle and avian furcula, with comments on the homology of dermal elements in the pectoral apparatus. J Exp Zool B Mol Dev Evol *314B*, 196–207. 10.1002/JEZ.B.21326.
- 440 15. Klima, M. (1973). Die Frühentwicklung des Schultergürtels und des Brustbeins bei den Monotremen (Mammalia: Prototheria). Adv. Anat. Embryol. Cell Biol. *47*, 1–80.
- 442 16. Lécuru S (1968). Étude des variations morphologiques du sternum, des clavicules, et de L'interclavicule des lacertiliens. Annales des Sciences Naturelles, Zoologie, Paris, 12th Série 10, 511–544.
- 445 17. Jones, M.E.H., Curtis, N., O'Higgins, P., Fagan, M., and Evans, S.E. (2009). The head and neck muscles associated with feeding in *Sphenodon* (Reptilia: Lepidosauria: Rhynchocephalia). Palaeontologia Electronica *12*, 12.2.7A.
- Howell, A.B. (1936). Morphogenesis of the Shoulder Architecture. Part IV. Reptilia. Q Rev Biol *11*, 183–208. 10.1086/394505.
- 450 19. Gambaryan, P.P., Kuznetsov, A.N., Panyutina, A.A., and Gerasimov, S. v. (2015).
 451 Shoulder girdle and forelimb myology of extant monotremata. Russ J Theriol *14*, 1–56.
 452 10.15298/rusitheriol.14.1.01.
- 453 20. Hall, B.K. (2001). Development of the clavicles in birds and mammals. Journal of Experimental Zoology 289, 153–161. 10.1002/1097-010X(20010215)289:3<153::AID-455 JEZ1>3.0.CO;2-O.

- 456 21. Cave, A.J.E. (1970). Observations on the monotreme interclavicle. J Zool *160*, 297–312. 10.1111/j.1469-7998.1970.tb03083.x.
- 458 22. Klima, M. (1987). Early development of the shoulder girdle and sternum in marsupials (Mammalia: Metatheria). Adv Anat Embryol Cell Biol *109*, 297–312.
- 460 23. Bickley, S.R.B., and Logan, M.P.O. (2014). Regulatory modulation of the T-box gene
 461 Tbx5 links development, evolution, and adaptation of the sternum. Proc Natl Acad Sci U
 462 S A 111, 17917–17922. 10.1073/pnas.1409913111.
- 24. Chen, J.M. (1952). Studies on the morphogenesis of the mouse sternum. I. Normal embryonic development. J Anat *86*, 373–37386.
- 465 25. Fell, H.B. (1939). The origin and developmental mechanics of the avian sternum. Philos 466 Trans R Soc Lond B Biol Sci 229, 407–463. 10.1098/RSTB.1939.0002.
- Gladstone, R.J., and Wakeley, C.P. (1932). The Morphology of the Sternum and its Relation to the Ribs. J Anat *66*, 508–564.
- Parker, W.K. (1868). A monograph on the structure and development of the shoulder-girdle and sternum in the Vertebrata (Robert Hardwicke) 10.5962/bhl.title.31928.
- 471 28. Musgrove, J. (1892). The costo-sternal articulations. J Anat Physiol 27, 1–4.
- 472 29. Chen, J.M. (1953). Studies on the morphogenesis of the mouse sternum. III. Experiments on the closure and segmentation of the sternal bands. J Anat 87, 130–149.
- 474 30. Durland, J.L., Sferlazzo, M., Logan, M., and Burke, A.C. (2008). Visualizing the lateral somitic frontier in the Prx1Cre transgenic mouse. J Anat 212, 590–602. 10.1111/j.1469-7580.2008.00879.x.
- 477 31. Nowicki, J.L., Takimoto, R., and Burke, A.C. (2003). The lateral somitic frontier: Dorsoventral aspects of anterio-posterior regionalization in avian embryos. Mech Dev *120*, 227–240. 10.1016/S0925-4773(02)00415-X.
- Shearman, R.M., and Burke, A.C. (2009). The lateral somitic frontier in ontogeny and phylogeny. J Exp Zool B Mol Dev Evol *312*, 603–612. 10.1002/jez.b.21246.
- 482 33. McIntyre, D.C., Rakshit, S., Yallowitz, A.R., Loken, L., Jeannotte, L., Capecchi, M.R., and Willik, D.M. (2007). Hox patterning of the vertebrate rib cage. Development *134*, 2981–2989. 10.1242/dev.007567.
- 485 34. Bi, W., Huang, W., Whitworth, D.J., Deng, J.M., Zhang, Z., Behringer, R.R., and De 486 Crombrugghe, B. (2001). Haploinsufficiency of Sox9 results in defective cartilage 487 primordia and premature skeletal mineralization. Proc Natl Acad Sci U S A *98*, 6698– 488 6703. 10.1073/pnas.111092198.
- 489 35. Sanford, L.P., Ormsby, I., Gittenberger-de Groot, A.C., Sariola, H., Friedman, R., Boivin,
 490 G.P., Cardell, E. lou, and Doetschman, T. (1997). TGFβ2 knockout mice have multiple
 491 developmental defects that are non-overlapping with other TGFβ knockout phenotypes.
 492 Development 124, 2659–2670. 10.1242/dev.124.13.2659.
- 493 36. Pizard, A., Burgon, P.G., Paul, D.L., Bruneau, B.G., Seidman, C.E., and Seidman, J.G. (2005). Connexin 40, a target of transcription factor Tbx5, patterns wrist, digits, and sternum. Mol Cell Biol *25*, 5073–5083. 10.1128/MCB.25.12.5073-5083.2005.
- 496 37. Smith-Paredes, D., Vergara-Cereghino, M.E., Lord, A., Moses, M.M., Behringer, R.R., and Bhullar, B.A.S. (2022). Embryonic muscle splitting patterns reveal homologies of amniote forelimb muscles. Nat Ecol Evol *6*, 604–613. 10.1038/s41559-022-01699-x.
- 499 38. Angielczyk, K.D., and Kammerer, C.F. (2018). 5. Non-Mammalian synapsids: the deep roots of the mammalian family tree. In Mammalian Evolution, Diversity and Systematics, pp. 117–198. 10.1515/9783110341553-005.
- 502 39. Lungmus, J.K., and Angielczyk, K.D. (2021). Phylogeny, function and ecology in the deep evolutionary history of the mammalian forelimb. Proceedings of the Royal Society B: Biological Sciences 288, 20210494. 10.1098/rspb.2021.0494.

- 505 40. Ruta, M., Botha-Brink, J., Mitchell, S.A., and Benton, M.J. (2013). The radiation of cynodonts and the ground plan of mammalian morphological diversity. Proceedings of the Royal Society B: Biological Sciences 280, 20131865. 10.1098/rspb.2013.1865.
- 508 41. Watson, D. (1917). The evolution of the tetrapod shoulder girdle and fore-limb. J Anat 52, 1–63.
- 510 42. Fahn-Lai, P., Biewener, A.A., and Pierce, S.E. (2018). Three-dimensional mobility and muscle attachments in the pectoral limb of the Triassic cynodont *Massetognathus* pascuali (Romer, 1967). J Anat 232, 383–406. 10.1111/joa.12766.
- 513 43. Regnault, S., and Pierce, S.E. (2018). Pectoral girdle and forelimb musculoskeletal function in the echidna (*Tachyglossus aculeatus*): Insights into mammalian locomotor evolution. R Soc Open Sci *5*, 181400. 10.1098/rsos.181400.
- Romer, A.S. (1922). The locomotor apparatus of certain primitive and mammal-like reptiles. Bull Am Mus Nat Hist *46*, 517–606.
- 518 45. Brocklehurst, R.J., Fahn-Lai, P., Regnault, S., and Pierce, S.E. (2022). Musculoskeletal modeling of sprawling and parasagittal forelimbs provides insight into synapsid postural transition. iScience 25. 10.1016/j.isci.2021.103578.
- 521 46. Bendel, E.M., Kammerer, C.F., and Fröbisch, J. (2019). Postcranial anatomy of a 522 gorgonopsian and its implications for the evolution of the mammalian sternum. Journal of 523 Morphology, Abstracts of the International Congress of Vertebrate Morphology *12*, S81.
- 524 47. Callison, W.É., Holowka, N.B., and Lieberman, D.E. (2019). Thoracic adaptations for ventilation during locomotion in humans and other mammals. Journal of Experimental Biology 222, jeb189357. 10.1242/jeb.189357.
- 527 48. Grey, H. (1966). Gray's Anatomy 28th ed. C. M. Goss, ed. (LEA & FEBIGER).
- 528 49. Margulies, S.S., Rodarte, J.R., and Hoffman, E.A. (1989). Geometry and kinematics of dog ribs. J Appl Physiol *67*, 707–712. 10.1152/jappl.1989.67.2.707.
- 530 50. de Troyer, A., Kirkwood, P.A., and Wilson, T.A. (2005). Respiratory action of the intercostal muscles. Physiol Rev *85*, 717–756. 10.1152/physrev.00007.2004.
- 532 51. Beyer, B., Feipel, V., Sholukha, V., Chèze, L., and van Sint Jan, S. (2017). In-vivo 533 analysis of sternal angle, sternal and sternocostal kinematics in supine humans during 534 breathing. J Biomech *64*, 32–40. 10.1016/j.jbiomech.2017.08.026.
- 535 52. Deméré, T.A., McGowen, M.R., Berta, A., and Gatesy, J. (2008). Morphological and molecular evidence for a stepwise evolutionary transition from teeth to baleen in mysticete whales. Syst Biol *57*, 15–37. 10.1080/10635150701884632.
- 538 53. Fordyce, R.E., and Marx, F.G. (2018). Gigantism Precedes Filter Feeding in Baleen Whale Evolution. Current Biology *28*, 1670–1676. 10.1016/j.cub.2018.04.027.
- 540 54. Geisler, J.H., Boessenecker, R.W., Brown, M., and Beatty, B.L. (2017). The Origin of Filter Feeding in Whales. Current Biology 27, 2036-2042.e2. 10.1016/j.cub.2017.06.003.
- 542 55. Marx, F.G., Tsai, C.H., and Fordyce, R.E. (2015). A new Early Oligocene toothed 543 "baleen" whale (Mysticeti: Aetiocetidae) from western North America: one of the oldest 544 and the smallest. R Soc Open Sci 2. 10.1098/RSOS.150476.
- 545 56. Peredo, C.M., Pyenson, N.D., Marshall, C.D., and Uhen, M.D. (2018). Tooth Loss Precedes the Origin of Baleen in Whales. Current Biology 28, 3992–4000. 10.1016/j.cub.2018.10.047.
- 548 57. de Muizon, C., Bianucci, G., Martínez-Cáceres, M., and Lambert, O. (2019). *Mystacodon selensis*, the earliest known toothed mysticete (Cetacea, Mammalia) from the late Eocene of Peru: anatomy, phylogeny, and feeding adaptations. Geodiversitas *41*, 401–499.
- 552 58. Peredo, C.M., and Uhen, M.D. (2016). A new basal chaeomysticete (Mammalia: 553 Cetacea) from the Late Oligocene Pysht Formation of Washington, USA. Pap Palaeontol 2, 533–554. 10.1002/spp2.1051.

- Kienle, S.S., Ekdale, E.G., Reidenberg, J.S., and Deméré, T.A. (2015). Tongue and
 Hyoid Musculature and Functional Morphology of a Neonate Gray Whale (Cetacea,
 Mysticeti, Eschrichtius robustus). Anatomical Record 298, 660–674. 10.1002/ar.23107.
- 558 60. Fitzgerald, E.M.G. (2010). The morphology and systematics of *Mammalodon colliveri*559 (Cetacea: Mysticeti), a toothed mysticete from the Oligocene of Australia. Zool J Linn Soc
 158, 367–476. 10.1111/j.1096-3642.2009.00572.x.
- 561 61. Boessenecker, R.W., and Fordyce, R.E. (2015). A new Eomysticetid (Mammalia: Cetacea) from the Late Oligocene of New Zealand and a re-evaluation of '*Mauicetus*' waitakiensis. Pap Palaeontol 1, 107–140. 10.1002/spp2.1005.
- 62. Brandt, J.F. (1873). Die fossilen und subfossilen Cetacea Europa's. Mémoires de L'Académie Impériale des Sciences de St.-Péetersbourg XX, 372.
- 566
 63. Gol'din, P., Startsev, D., and Krakhmalnaya, T. (2013). The Anatomy of the Late Miocene
 567 Baleen Whale *Cetotherium riabinini* from Ukraine. Acta Palaeontol Pol *59*, 795–814.
 568 10.4202/app.2012.0107.
- 569 64. Brown, R.E., and Butler., J.P. (2000). The absolute necessity of chest-wall collapse during diving in breath-hold diving mammals. Aquat Mamm *26*, 26–32.
- 571 65. Fahlman, A., Moore, M.J., and Garcia-Parraga, D. (2017). Respiratory function and mechanics in pinnipeds and cetaceans. Journal of Experimental Biology *220*, 1761–1773. 10.1242/JEB.126870.
- 574 66. Fahlman, A., Loring, S.H., Levine, G., Rocho-Levine, J., Austin, T., and Brodsky, M. (2015). Lung mechanics and pulmonary function testing in cetaceans. Journal of Experimental Biology *218*, 2030–2038. 10.1242/jeb.119149.
- 577 67. Lillie, M.A., Piscitelli, M.A., Vogl, A.W., Gosline, J.M., and Shadwick, R.E. (2013).
 578 Cardiovascular design in fin whales: high-stiffness arteries protect against adverse
 579 pressure gradients at depth. Journal of Experimental Biology *216*, 2548–2563.
 580 10.1242/jeb.081802.
- 581 68. Pabst DA, Rommel SA, and McLellan WA (1999). Functional anatomy of marine mammals. In Biology of Marine Mammals, J. Reynolds III and S. Rommel, eds. (Smithsonian Institution Press), pp. 15–72.
- 584 69. Rommel, S.A., Costidis, A.M., Fernandez, A., Jepson, P.D., Pabst, D., Mclellan, W.A., 585 Houser, D.S., Cranford, T.W., van Helden, A.L., Allen, D.M., et al. (2006). Elements of 586 beaked whale anatomy and diving physiology and some hypothetical causes of sonarrelated stranding. J. Cetacean Res. Manage 7, 189–209.
- 588 70. Slijper, E.J. (1936). Die Cetaceen, vergleichen-anatomisch und systematisch (M. Nijhoff).
- 589 71. Goldbogen, J.A., Friedlaender, A.S., Calambokidis, J., McKenna, M.F., Simon, M., and 590 Nowacek, D.P. (2013). Integrative Approaches to the Study of Baleen Whale Diving 591 Behavior, Feeding Performance, and Foraging Ecology. Bioscience 63, 90–100. 592 10.1525/bio.2013.63.2.5.
- 593 72. Friedlaender, A.S., Bowers, M.T., Cade, D., Hazen, E.L., Stimpert, A.K., Allen, A.N.,
 594 Calambokidis, J., Fahlbusch, J., Segre, P., Visser, F., et al. (2020). The advantages of
 595 diving deep: Fin whales quadruple their energy intake when targeting deep krill patches.
 596 Funct Ecol 34, 497–506. 10.1111/1365-2435.13471.
- 597 73. Goldbogen, J.A., Cade, D.E., Calambokidis, J., Friedlaender, A.S., Potvin, J., Segre, P.S., and Werth, A.J. (2017). How Baleen Whales Feed: The Biomechanics of Engulfment and Filtration. Ann Rev Mar Sci 9, 367–386. 10.1146/annurev-marine-122414-033905.
- 601 74. Krauß-Hoeft C (1978). Morphogenese und Ossifikation des Sternum bei den Cetacea. Inaug. Diss. Frankfurt a.M.
- 603 75. Stahl, W.R. (1967). Scaling of respiratory variables in mammals. J Appl Physiol 22, 453–460. 10.1152/jappl.1967.22.3.453.

- 605 76. Kahane-Rapport, S.R., and Goldbogen, J.A. (2018). Allometric scaling of morphology and engulfment capacity in rorqual whales. J Morphol 279, 1256–1268. 10.1002/jmor.20846.
- Goldbogen, J.A., Shadwick, R.E., Lillie, M.A., Piscitelli, M.A., Potvin, J., Pyenson, N.D., and Vogl, A.W. (2015). Using morphology to infer physiology: case studies on rorqual whales (Balaenopteridae). Can J Zool *93*, 687–700. 10.1139/cjz-2014-0311.
- 510 78. Stovall, J.W., Price, L.I., and Romer, A.S. (1966). The postcranial skeleton of the giant Permian pelycosaur *Cotylorhynchus romeri*. Bulletin of the Museum of Comparative Zoology *135*, 1–30.
- 613 79. Gaetano, L.C., Mocke, H., and Abdala, F. (2018). The postcranial anatomy of
 614 Diademodon tetragonus (Cynodontia, Cynognathia). J Vertebr Paleontol 38, e1451872.
 615 10.1080/02724634.2018.1451872.
- 616 80. Morris, H., and Jackson, C.M. (1933). Morris' Human Anatomy: A Complete Systematic Treatise. (P. Blakiston).
- 618 81. Logan, M., Martin, J.F., Nagy, A., Lobe, C., Olson, E.N., and Tabin, C.J. (2002).
 619 Expression of Cre Recombinase in the developing mouse limb bud driven by a Prxl
 620 enhancer. Genesis 33, 77–80. 10.1002/gene.10092.
- 621 82. Madisen, L., Zwingman, T.A., Sunkin, S.M., Oh, S.W., Zariwala, H.A., Gu, H., Ng, L.L., 622 Palmiter, R.D., Hawrylycz, M.J., Jones, A.R., et al. (2010). A robust and high-throughput 623 Cre reporting and characterization system for the whole mouse brain. Nat Neurosci *13*, 624 133–140. 10.1038/nn.2467.
- 83. Jukkola, T., Trokovic, R., Maj, P., Lamberg, A., Mankoo, B., Pachnis, V., Savilahti, H.,
 626 and Partanen, J. (2005). Meox1Cre: A mouse line expressing Cre recombinase in somitic
 627 mesoderm. Genesis 43, 148–153. 10.1002/gene.20163.
- Lufkin, T., Mark, M., Hart, C.P., Dollé, P., LeMeur, M., and Chambon, P. (1992).
 Homeotic transformation of the occipital bones of the skull by ectopic expression of a homeobox gene. Nature 359, 835–841. 10.1038/359835a0.
- 631 85. McGlinn, E., Holzman, M.A., and Mansfield, J.H. (2019). Detection of Gene and Protein Expression in Mouse Embryos and Tissue Sections. Methods Mol Biol *1920*, 183–218. 10.1007/978-1-4939-9009-2_12.
- 634 86. Philippidou, P., Walsh, C.M., Aubin, J., Jeannotte, L., and Dasen, J.S. (2012). Sustained Hox5 gene activity is required for respiratory motor neuron development. Nat Neurosci 15, 1636–1644. 10.1038/nn.3242.
- 637 87. Gould, A., Morrison, A., Sproat, G., White, R.A., and Krumlauf, R. (1997). Positive cross-638 regulation and enhancer sharing: two mechanisms for specifying overlapping Hox 639 expression patterns. Genes Dev *11*, 900–913. 10.1101/gad.11.7.900.

640

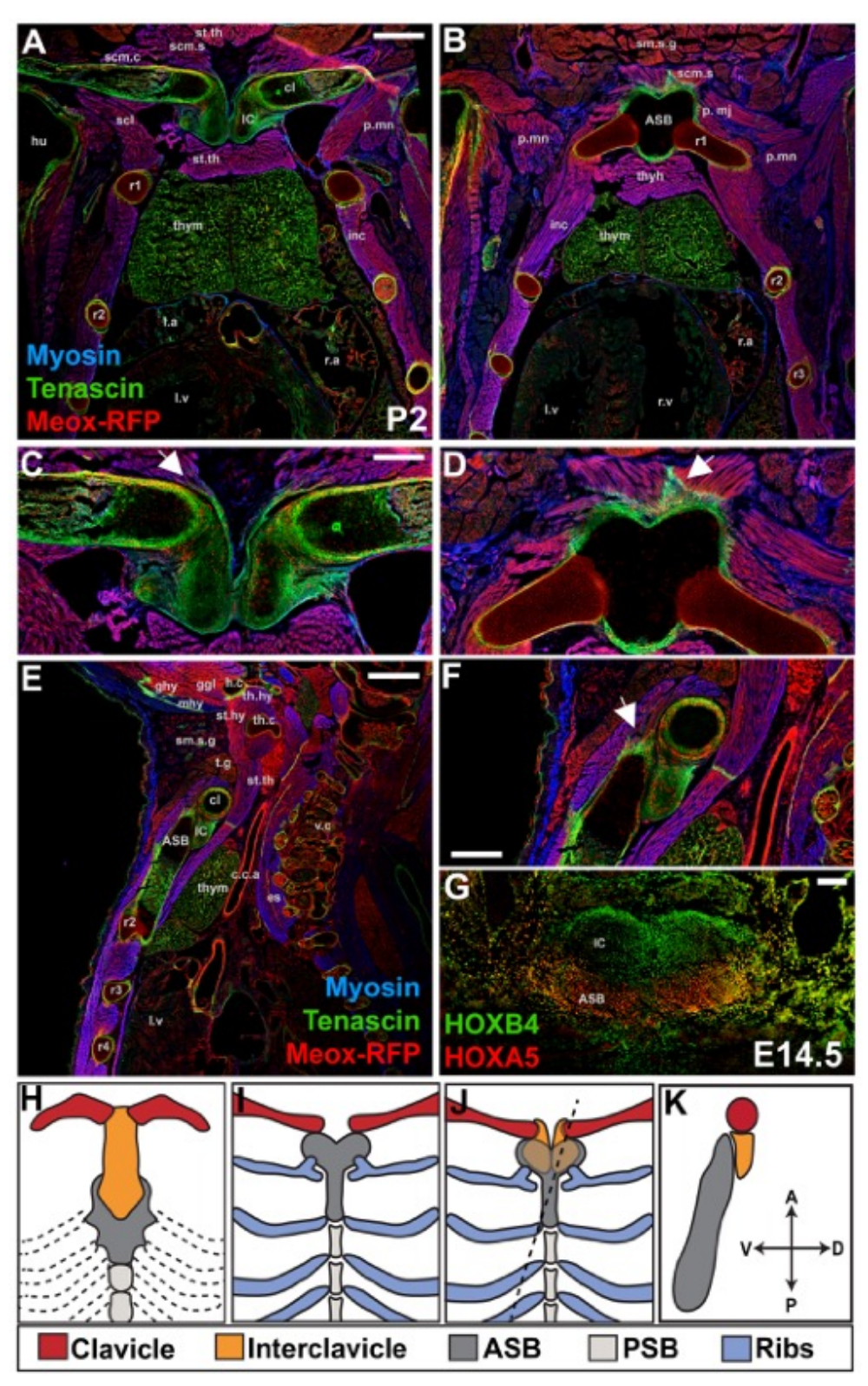


Figure 1. The mouse presternum is composed of two bilateral elements that are morphologically and molecularly distinct.

(A-F) Expression of tenascin (green), muscle myosin (blue), and Meox1-Cre-dependent RFP (red) in P2 mouse pups, in either frontal (A-D) or sagittal (E-F) views, reveals that the mouse presternum comprises two major elements, IC and ASB. Meox1-Cre-dependent RFP is used as a lineage-label for cells derived from somites, which include skeletal muscle and ribs. Note that overlap of tenascin and Meox1-Cre-RFP appears yellow; overlap of myosin and Meox-RFP appears purple. (C,D,F) show higher magnification views of (A,B,E), respectively. Arrows indicate Tenascin-expressing attachment of the sternocleidomastoid muscle to the interclavicle (C) and the anterior sternal bars (D,F). (G) Expression of HOXA5 (red), and HOXB4 (green) in transverse sections of E14.5 embryos, reveals unique molecular identity of IC and ASB. Note that HOXA5/HOXB4 colocalization appears yellow. (H-K) Diagrams comparing skeletal structure and proposed homologies in a non-therian outgroup (H, a gorgonopsian, redrawn from ³), with the previous model for therians (I, mouse), and the proposed new model for therians (J-K, mouse in frontal and sagittal views respectively). (J-K) are drawn from micrographs shown in panels (A) and (E). Dashed line in (J) indicates the approximate section plane of the specimen shown in (E). Scale bars: A,B,E, 400mM; C,D,F, 200mM; G, 100mM. Abbreviations: ASB, anterior sternal bands; IC, interclavicle; r1,2,3, rib 1,2,3. For a full list of abbreviations see the Figure S1 legend. See also Figures S1, S2, and S3.

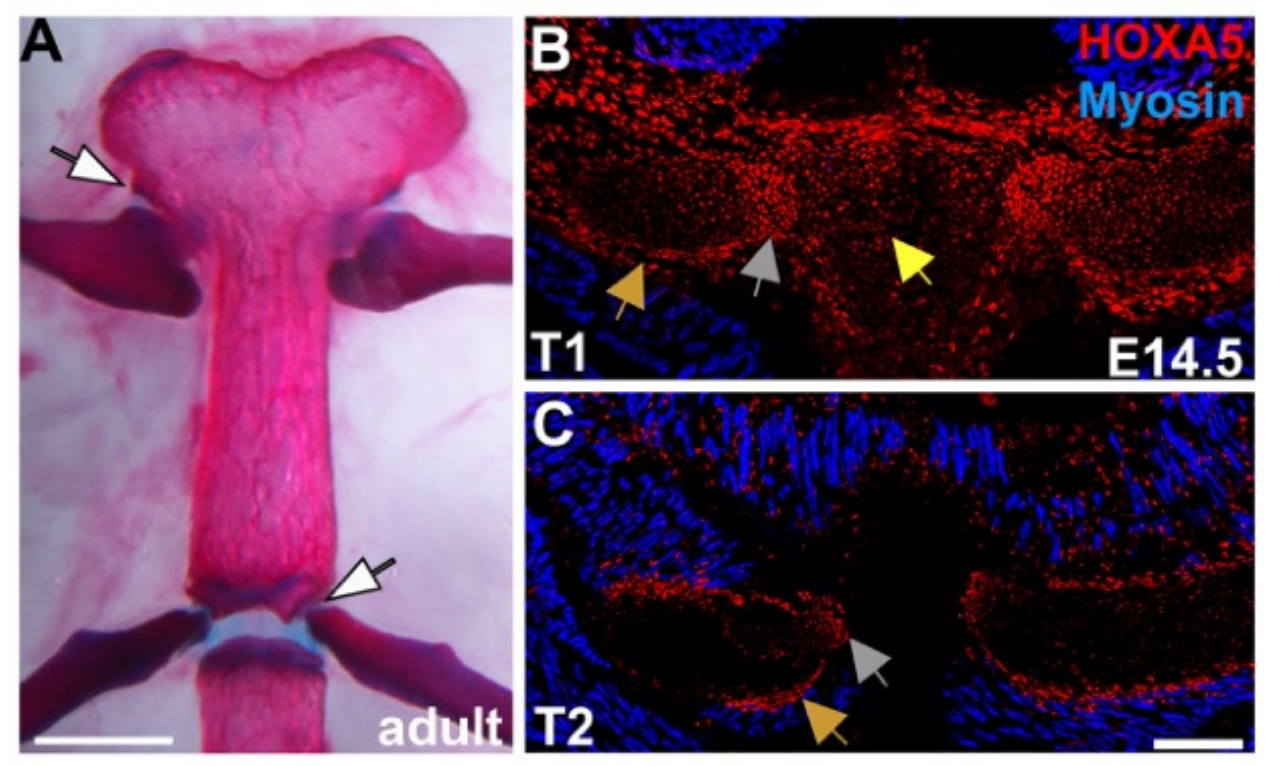


Figure 2. Unique morphology and embryonic gene expression of the T1 costosternal joint.

(A) Adult mouse sternum presenting ventral view of T1 and T2 costosternal joints. Note that the clavicles and IC have been removed. (B-C) Expression of HOXA5 (red), and muscle myosin (blue) at the T1 (B) or T2 (C) costosternal joint, in transverse sections of E14.5 embryos. Orange arrows indicate HOXA5 expression in the rib perichondrium; gray arrows point to HOXA5 expression in the rib tip where sternal attachment occurs. Note the highest expression of HOXA5 occurs in the rib perichondrium and in chondrocytes where they contact the sternal bands. Yellow arrow in (B) indicates HOXA5 expression in the ASB at the level of T1 attachment. This expression is notably absent throughout the PSB, shown at T2 (B). Scale bars: A, 1mm, B-C, 200mM. Abbreviations: T1, thoracic rib 1; T2, thoracic rib 2. See also Figures S2 and S3.

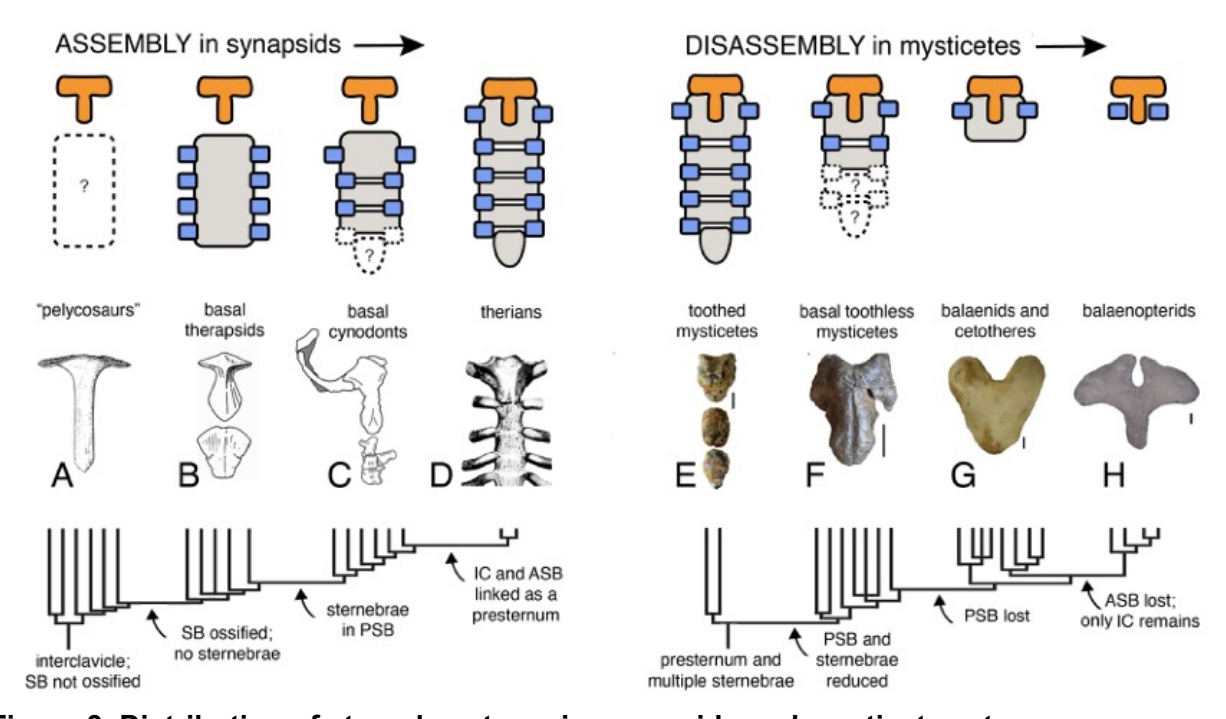


Figure 3. Distribution of sternal anatomy in synapsids and mysticete cetaceans. Synapsids (left panel) and mysticete cetaceans (right panel). Bottom row: consensus phylogenies modified from ³⁸ (synapsids) and ⁵⁸ (mysticete cetaceans). Middle row, sternal anatomy. Line drawings of fossil synapsids were taken from the literature and modified to show only the interclavicle and sternal bands. (A) The pelycosaur *Cotylorhynchus romeri*⁷⁸; (B) the basal therapsid *Dicynodon* sp. ⁴¹; (C) the basal therapsid *Diademodon tetragonus*⁷⁹; (D) the therian *Homo sapiens*⁸⁰. Not to scale. Photographs of mysticete sterna: (E) the late Eocene toothed mysticete *Mystacodon selensis* from ⁵⁷, modified by posterior truncation of the mesosternum and xiphisternum; (F) The Late Oligocene toothless mysticete *Sitsqwayk cornishorum* UWBM VP82916; (G) the balaenid *Eubalaena glacialis* USNM 593893; (H) The balaenopterid *Balaenoptera physalus* MCZ 35887. All scale bars = 5 cm. Top row: hypothesis of assembly and disassembly of elements in the therian sternum presented diagrammatically. Colors: orange, interclavicle; gray = sternal bands; blue = ribs. Abbreviations: ASB = anterior sternal bands, IC = interclavicle, PSB = posterior sternal bands, SB = sternal bands. See also Figure S3.

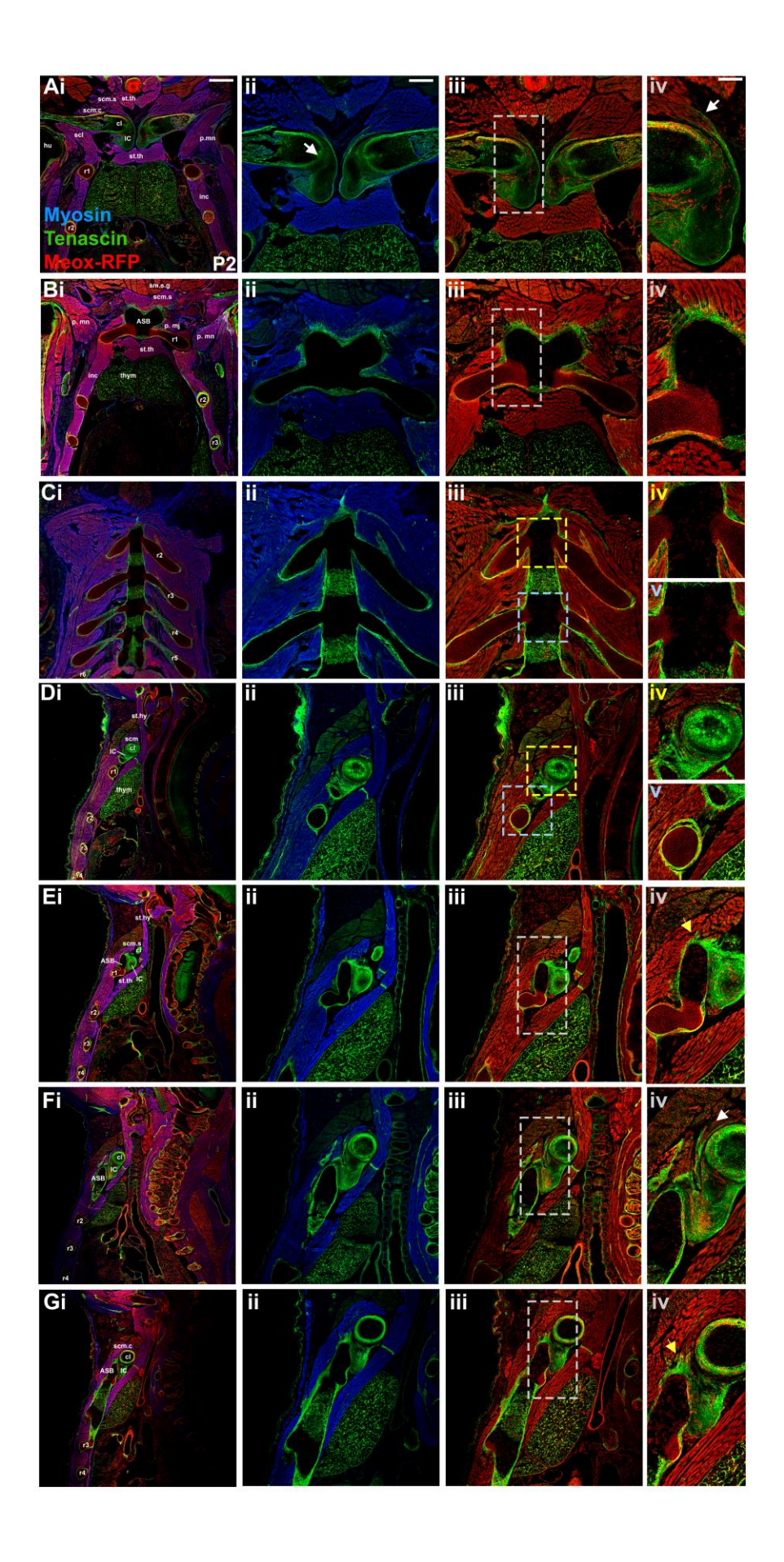


Figure S1. Composite nature of the mouse presternum, Related to Figure 1.

(Ai-Giv) Expression of Tenascin (green), muscle Myosin (blue), and Meox1-Cre-RFP (red) in P2 mouse pups, in either frontal (Ai-Cv) or sagittal (Di-Giv) views, reveals that the mouse presternum comprises multiple elements. (A-C) successive sections progressing ventrally. (D-G) Successive sections progressing from lateral right clavicle (D), to the midline (E), and then continuing laterally to the left clavicle (F, G). Overlap of Tenascin and Meox1-Cre-RFP, yellow: overlap of Myosin and Meox1-Cre-RFP, purple. All muscles are somite-derived, hence purple in (Ai). (Aii-Giii) show higher magnification views of (Ai-Gi); Aiv-Giv show higher magnification views of (Aiii-Giii). Boxes in (Aiii-Giii) indicate region depicted in (Aiv-Giv). In frontal views, progressing dorsal to ventral, the first presternal element to appear is the IC (Ai-Aiv). Tenascin expression marks the clavicles, IC, ribs, and muscle insertions. The IC presents as a bilateral element, with attachments laterally to the clavicles (Ai-iii). A line of Tenascin expression marks the boundary between clavicles and IC (arrow in Aii). The appearance of somite-derived, Meox-RFP cells in the clavicle and IC may indicate the presence of somite-derived osteoclasts during bone maturation (Aii-iv). Tenascin marks the attachment point of the sternocleidomastoid muscle to the anterior IC (arrow in Aiv). Progressing ventrally, a frontal section reveals a second, Y-shaped component of the presternum, the ASB, slightly posterior to the IC (Bi-iii). The first rib is seen attaching to the base of the Y (Bi-iii). While some Meox1-Cre-RFP cells can be visualized as scattered in the sternum at this stage, the lateral somitic frontier is clearly delineated as the site of rib 1- sternum fusion (Biv). Tenascin indicates ASB attachments anteriorly to the sternocleidomastoid muscle, and laterally to the pectoralis muscle (Bii-iv). (Ci-iii) A frontal section through the sternum posterior to rib 1 shows organization of the sternebrae, with inhibition of osteogenesis at sites of rib attachment. Meox-RFP expression discloses the LSF as a boundary at the site of rib contact (Ciii-v). Some Meox-RFP cells appear to populate the sternum at this postnatal stage (Civ-v). In sagittal view, the relative positioning of the two elements comprising the presternum is apparent, with the IC sitting dorsal and anterior (Di-Giii) to the ASB. Continuity between the ventral posterior element and the rest of the sternum suggests that this portion of the presternum consists of the ASB (Di-Giii). Arrows in (Fiv) and (Giv) indicate attachment of the sternocleidomastoid muscle to IC and ASB, respectively. Scale bars: Ai-Gi, 400µm; Aii-Giii, 200µm; Aiv-Giv, 100µm. Abbreviations: ASB, anterior sternal bands; c.c.a, common carotid artery; cl, clavicle; es, esophagus; ggl, genioglossus muscle; ghy, geniohyoid muscle; h.c, hyoid cartilage; hu, humerus; IC, interclavicle; inc, intercostal muscle; I.a, left atrium; I.v, left ventricle; mhy, mylohyoid muscle; p.mj, pectoralis major muscle; p.mn, pectoralis minor muscle; r1,2,3, rib 1,2,3; r.a, right atrium; r.v, right ventricle; scl, subclavius muscle; scm.c, clavicular head of the sternocleidomastoid muscle; scm.s, sternal head of the sternocleidomastoid muscle; sm.s.g, submandibular salivary gland; st.hy, sternohyoid muscle; st.th, sternothyroid muscle; th.c, thyroid cartilage; t.g, thyroid gland; thym, thymus; thhy, thyrohyoid muscle; v.c., vertebral column.

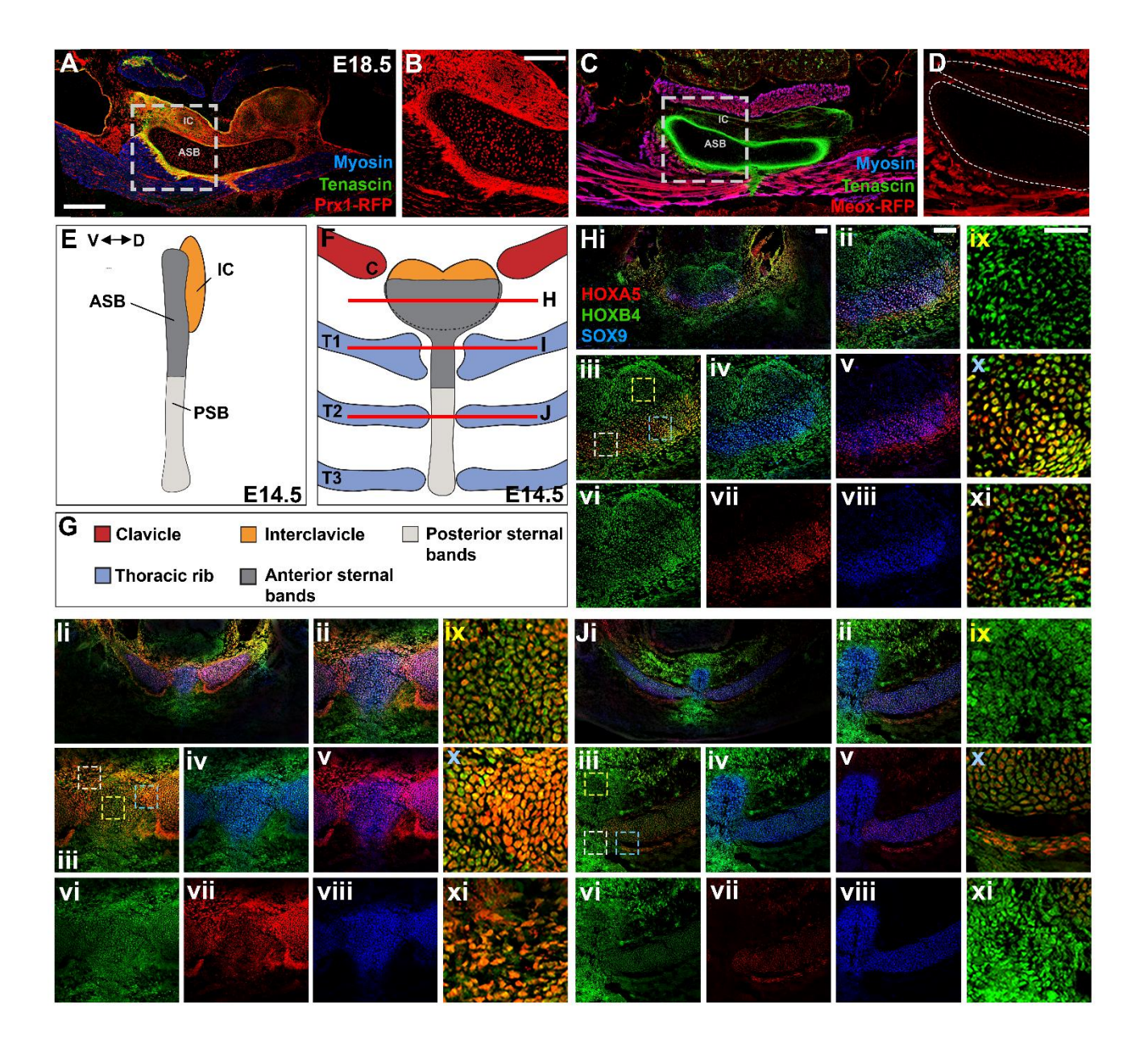


Figure S2. Both the IC and ASB are derived primarily from lateral plate mesoderm, but each component of the embryonic mouse presternum is molecularly distinct. Related to Figures 1-2.

(A-D) Lineage labeling allowed tracking of cells derived from somites (including ribs and skeletal muscle) or lateral plate mesoderm (LPM) using Meox1-Cre or Prx1-Cre-dependent expression of RFP. (A-B) Expression of Tenascin (green), muscle Myosin (blue), and Prx1-Cre-RFP (red) in transverse sections of E18.5 embryos reveals extensive labeling of both the IC and ASB. (C-D) Expression of Tenascin (green), muscle Myosin (blue), and Meox1-Cre-RFP (red) in transverse sections of E18.5 embryos, shows near-absence of somite-derived cells in both IC and ASB. Regions of (A) and (C) indicated by dotted lines are magnified in (B) and (D) respectively. (E-G) Schematic illustrating the components of the mouse presternum at E14.5, in side (E) or front (F) views. The IC is located dorsal to and extends further anteriorly than the ASB; both elements overlap in the presternum, and the posterior border of the IC is anterior to the T1 attachment. The clavicles articulate with the lateral sides of the IC, the T1 ribs articulate with the ASB, and the ASB is continuous with the rest of the sternum, or PSB. Red lines in (F) indicate the anterior-posterior level of images shown in (H-J). (H-J) HOX expression distinguishes the IC and ASB. Each panel is organized as follows: (i) Expression of HOXA5 (red), HOXB4 (green), and SOX9 (blue) in transverse sections of E14.5 embryos. Co-expression of HOXA5 and HOXB4, yellow; co-expression of HOXA5 and SOX9, purple; co-expression of HOXB4 and SOX9, cyan. (ii-viii) are magnified views of (i), showing expression subsets as follows: (ii), HOXA5, HOXB4, SOX9; (iii), HOXA5, HOXB4; (iv), HOXB4, SOX9; (v), HOXA5, SOX9; (vi), HOXB4; (vii), HOXA5; (viii), SOX9. Higher magnification views of boxed areas in (iii) are shown in: (ix), yellow box; (x), blue box; (xi), white box. At all axial levels (H-J), SOX9 labels cartilage cells in the IC. ASB, PSB, and ribs, Expression of SOX9 in the IC is weaker and more diffuse than in the rest of the sternum (for example, compare panels in H, where the yellow boxed area of Hiii is within the IC and the blue boxed area is within the ASB). (Hi-ii) Anterior to the rib 1 attachment, HOXB4 is expressed throughout the IC and ASB, while HOXA5 is restricted only to the ASB. Shown in further detail, the IC expresses HOXB4 and SOX9 but not HOXA5 (Hiii-ix). In contrast, HOXB4 and HOXA5 are co-expressed with SOX9 in the ASB (Hiii-viii; x). Further, while HOXB4 expression is high throughout the ASB (Hx, xi), HOXA5 shows medial exclusion such that many cells co-express HOXA5 and HOXB4 laterally (Hx) but only a handful coexpress both medially (Hxi). (Ii-ii) At the axial level of the rib 1 attachment, the IC is not present, and the ASB shows the more rounded morphology characteristic of the posterior sternum. SOX9 marks both the ASB and T1 rib (li.viii). There is considerable overlap between HOXA5 and HOXB4 expression in the T1 rib (liii-viii x), particularly in the rib perichondrium (li, v, vi), and there is also overlap in the ASB (Iiii-viii; ix). HOXA5 and HOXB4 are also co-expressed in a population of cells dorsal to the ribs and ASB (Ixi). At the level of rib 2 attachment (Ji-ii), expression of HOXB4 remains high in both the PSB (Jiii-viii, ix, xi) and T2 ribs (Jiv, vi, x). In contrast, HOXA5 is expressed in the T2 rib (Jiii-viii,x), but is not present in the PSB (Jiii-viii; xi). Scalebars: A,C, 400µm; B,D, 200µm; H-J i-viii, 100µm; ix-xi, 50µm. Abbreviations: ASB, anterior sternal bands; IC, interclavicle; PSB, posterior sternal bands; T1, first thoracic rib; T2, second thoracic rib.

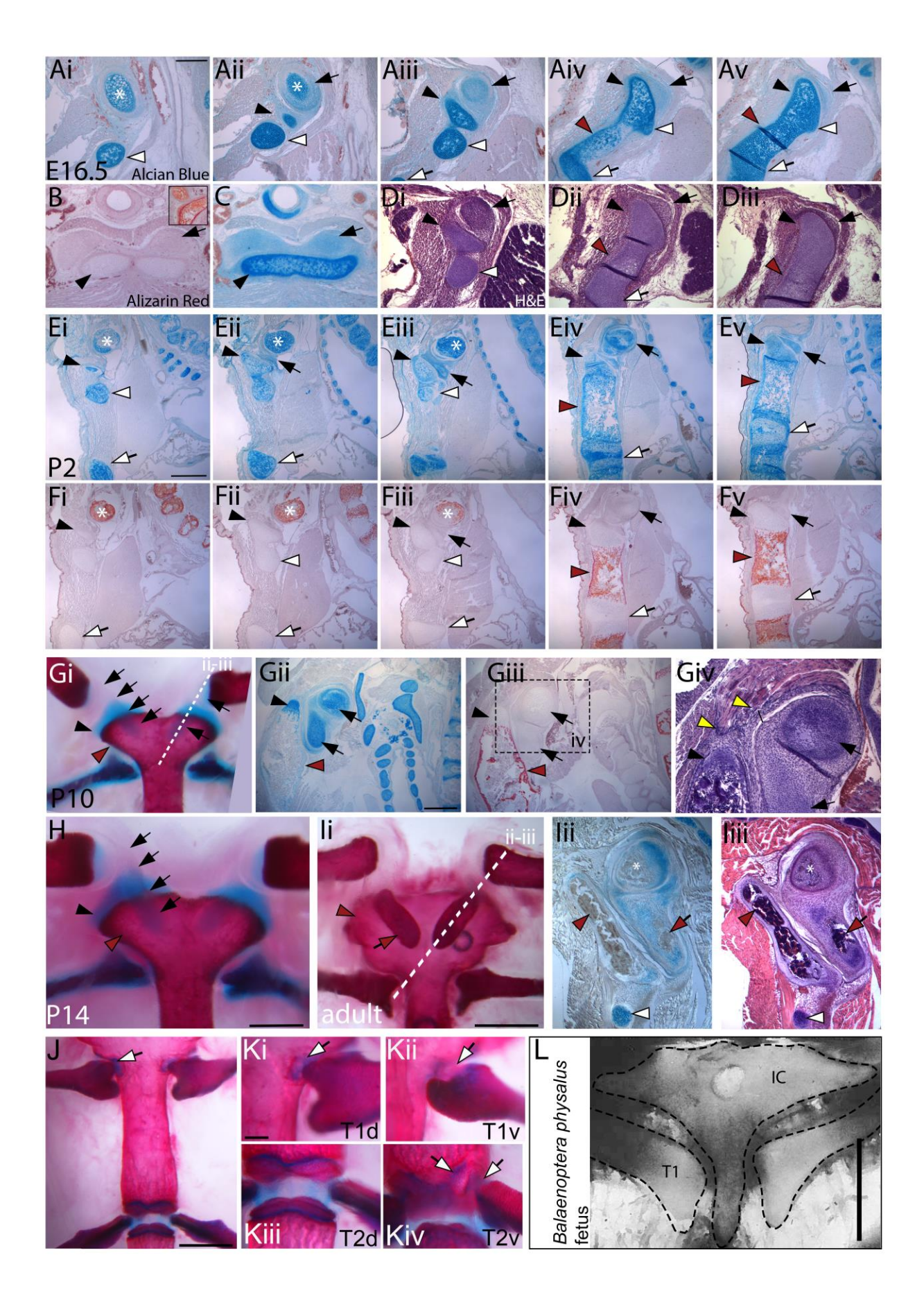


Figure S3. Histological analysis of sternal components. Related to Figures 1-3.

All sections are sagittal with anterior up and dorsal to the right except (B-C), which are transverse with dorsal up. Sagittal sections shown in A,D,E and F move in series along a row from lateral (left panels) toward the midline (right-most panels). At E16.5 (A-D), the clavicle (asterisks), sternal bands (black arrowheads), and rib 1 (white arrowhead) are composed of chondrocytes in a cartilage matrix stained strongly with Alcian blue (A-C). In contrast, the interclavicle (black arrows) is only weakly Alcian blue positive (Aii-v, C). The regions of the sternal bands that will ossify (red arrowheads) contain enlarged, hypertrophic chondrocytes (Aiv-v, Dii-iii), but these have not yet mineralized (B, and data not shown). Inset in B shows an Alizarin Red- positive vertebral ossification from the same section). The clavicles appear to be wrapped in interclavicle at their medial ends, such that the clavicle appears to grade into the interclavicle (Ai-iii). The interclavicle alone (without clavicle) is present in the most midline sections, where the distinct histology of interclavicle vs. ASB is most apparent (Aiii-v, C). (E-F) Show a similar series of sections at P2, symbols as above. The ribs and the sternum at points of rib attachment remain cartilaginous (E), but the sternebrae have begun to ossify, including the region between Ribs 1 and 2 attachment points (red arrowheads, Fiv-v). In contrast, the interclavicle continues to stain weakly with Alcian blue but not with Alizarin Red (Eiii-v, Fiii-v). Later in postnatal development, as seen in whole-mount at P10 (Gi) or P14(H), or in section (at P10, Gii-iv), a region of the IC (black arrows) has progressed toward endochondral ossification based on strong Alcian blue staining and the presence of round, proliferating chondrocytes. The chondrified area of the IC is limited to the rod-shaped posterior-lateral region, while the anterior-medial IC is not chondrified based on persistently weak Alcian blue staining and absence of round, proliferating chondrocytes. The IC has not ossified, based on absence of Alizarin red staining, at any stages shown, or prior to P30 (specimens examined at P16, P21 and P30, not shown, resemble P10-P14 shown here). The dotted line in (Gi) shows the approximate plane of section for the specimen shown in (Gii-iv). The attachment of the sternocleiomastoid to both the IC and SB can be seen (Giv, yellow arrowheads). (I) Morphology of the adult mouse presternum shown in whole-mount dorsal view (Ii) with the clavicles and IC attached or in sections (lii-iii) at approximately the plane indicated by the white dotted line in (li) and stained for Alican Blue (Iii) or H&E (Iiii). As above, asterisks mark the clavicle; red arrows mark the ossified region of the IC, red arrowheads mark the now fully ossified ASB, and white arrowheads mark Rib 1. Together, these reveal that a posterior, bilateral rod-shaped portion of the IC has ossified, while the anterior portion of the IC does not undergo skeletal differentiation and instead remains weakly Alcian Blue positive and Alizarin Red negative. Symbols for panels A-I are as follows: Asterisks mark the clavicle; black or red arrows mark the interclavicle before and after ossification; black or red arrowheads mark the ASB before or after ossification; white arrowheads mark Rib 1 or its attachment point on the sternum; white arrows mark Rib 2 or its attachment point on the sternum; red arrowheads mark the ossified sternebra that separates ribs 1-2. (J-K) Morphology of the adult rib articulations. (J) Dorsal view of an adult mouse sternum shows T1 and T2 costosternal joints. The clavicles and IC have been removed from this specimen. (Ki-iv) Higher magnification views from dorsal (d) and ventral (v) sides of T1 and T2 costosternal joints as labelled. Cartilaginous connections between the ribs and sternum shown in J-K are indicated by white arrows. At T1, the distal rib bifurcates, and its anterior tip is connected by synchondrosis to the ossified ASB. The posterior rib tip remains free, lying opposite a depression on the presternum. At T2, the distal rib tip retains a cartilaginous connection to sternum anterior to the sternebral joint, visible in ventral view. The sternum segments to form a synovial joint at the site of articulation. T3 and more posterior costosternal joints resemble T2 although they grade smaller as they progress posteriorly (not shown). (L) Relationship of the T1 Rib and sternum in balaenopterids. Relative positions of the distal T1 ribs and the "wings" of the sternum in a cleared 40cm long fetus of the balaenopterid mysticete Balaenoptera physalus, from S1. Dashed lines around the ribs and sternum have been overlaid

onto the original image. IC: interclavicle; T1, first thoracic rib. Scale bars: A-D, Giv, 250μm; E-F, 500μm; H, Gi, 500μm; Gii,iii, 500μm. I, 1mm; J, 1mm; Ki-iv, 250μm; L, 1 cm.

Supplemental Reference

S1. Krauß-Hoeft, C., 1978. Morphogenese und Ossifikation des Sternum bei den Cetacea. Inaug. Diss. Frankfurt a.M.